Boron-Vacancy Pairing and Its Effect on the Electronic Properties of Carbon Nanotubes

Kyoung E. Kweon, Gyeong S. Hwang and Yong-Hoon Kim

ECS Solid State Lett. 2012, Volume 1, Issue 4, Pages M19-M23.
doi: 10.1149/2.009203ssl

ECS Solid State Letters, **1** (4) M19-M23 (2012)
2162-8742/2012/1(4)/M19/5/$28.00 © The Electrochemical Society

Boron-Vacancy Pairing and Its Effect on the Electronic Properties of Carbon Nanotubes

Kyoung E. Kweon,[a] Gyeong S. Hwang,[a,z] and Yong-Hoon Kim[b]

[a]*Department of Chemical Engineering, University of Texas at Austin, Austin, Texas 78712, USA*
[b]*Graduate School of EEWS (WCU), KAIST, Taejon 305701, South Korea*

We examined the effect of B-V pairing on the electrical conductivity and electronic properties of CNTs, compared to isolated V and substitutional B cases. Using DFT calculations we first looked at the interaction of a mobile V with substitutional B in armchair CNTs with different tube diameters. NEGF-DFT calculations were then performed to determine the electronic structure and electrical conductivity of (5, 5) CNTs with an *V*, B_s, or B_s-*V*. Our study unequivocally demonstrates that upon B-V pairing vacancy-related features mostly disappear in the tube conductance, which turns out to be due to the passivation of V dangling bonds.
 [DOI: 10.1149/2.009203ssl]

Manuscript submitted May 3, 2012; revised manuscript received June 25, 2012. Published August 22, 2012.

Over the years considerable efforts have been undertaken to take advantage of the unique electrical, mechanical, and thermal properties of carbon nanotubes (CNTs) for the development of energy storage and conversion devices, sensors, and transistors.[1–4] It is well known that the electronic properties of CNTs are determined by the tube diameter and chirality.[1] In addition, many attempts have been made to tailor their electronic properties by introducing various chemical impurities.[5–7]

Boron is one of the most important substitutional dopants for sp^2-bonded carbon materials because of their comparable atomic size with carbon. Boron has one less valence electron than carbon, which can allow for a substantial modification of the electronic and magnetic properties of graphitic systems.[5,8–10] The substitutional doping of boron in CNTs may allow the selective sensing of NO_2 and NH_3 gases, better Li storage as a battery anode, and enhanced H storage.[11–13] Besides dopants, earlier high-resolution transmission electron microscopy (HR-TEM) measurements have provided evidence of the existence of vacancy-related defects[14,15] that modify the electronic structure of CNTs to a large extent. The effects of vacancy defects and substitutional dopants on the electrical conductance of CNTs have been rather well studied.[16–18] However, single vacancies may undergo migration in a CNT with moderate activation energy,[14,19] possibly leading to the formation of dopant-vacancy complexes that would cause a different electrical behavior from their "pure" counterparts (vacancies and dopants). Despite the importance, some fundamental aspects of the nature and formation of dopant-vacancy complexes and their influence on the electrical properties of CNTs remain unclear.

In this work, using combined density-functional theory (DFT) and nonequilibrium Green's function (NEGF) calculations we examine the formation, structure, and stability of a boron-vacancy pair in armchair CNTs with different diameters, and how the boron-vacancy pairing modifies the CNTs' electronic and charge transport properties with comparisons to isolated vacancy and boron cases. The improved understanding could offer insight into the tailoring of the properties of CNTs through impurity doping and defect engineering.

Calculation Methods

All the geometry optimization and energy calculations reported herein were performed on the basis of the spin-polarized DFT within the Perdew-Burke-Ernzerhof (PBE) generalized gradient approximation (GGA),[20] as implemented in the Vienna *ab-initio* Simulation Package (VASP).[21] The projector augmented wave (PAW) method with a planewave basis set was used to describe the interaction between ion cores and valence electrons.[22] An energy cutoff of 408 eV was applied for the planewave expansion of the electronic eigenfunctions. CNT structures were modeled using periodic boundary conditions in all three directions; each supercell contains a CNT with 10 unit cells (corresponding to 24.7 Å long according to the DFT-GGA-PBE) in the tube axis and has a vacuum space of 10 Å (perpendicular to the tube axis) between the (periodic image) tubes to avoid their unphysical interactions. All atoms were fully relaxed until residual forces on constituent atoms became smaller than 3×10^{-2} eV/Å. For Brillouin-zone integration, we employed a $(1\times1\times3)$ *k*-point mesh in the scheme of Monkhorst-Pack.[23]

The electronic transport properties were investigated using the fully self-consistent DFT-based NEGF method, as implemented in the TranSIESTA code.[24] As illustrated in Fig. 1, the calculation system is composed of a central scattering region and two semi-infinite electrodes. For a defective system, a defect or impurity was introduced in the scattering region which should be made long enough to screen the defect-induced scattering potential; in our calculations, the axial lengths of the scattering region and each electrode were set to 34.58 Å and 4.94 Å (corresponding to 14 units and 2 units), respectively. The electron conductance through a CNT at energy E and external bias V can be expressed by the product of the conductance quantum (per spin) ($= e^2/h$) and the transmission probability, i.e., $G(E,V) = g_0 T(E,V)$.[25] Within the framework of NEGF, $T(E,V)$ is given by $T(E,V) = Tr[\Gamma_L(E,V)G^R(E,V)\,\Gamma_R(E,V)G^A(E,V)]$,[26] where G^R (G^A) represents the retarded (advanced) Green's function of scattering region and coupling matrix Γ_L (Γ_R) between the left (right) electrode and the scattering region is the imaginary parts of the self-energy.[27] Here, the spin-polarized DFT calculations were performed within the GGA-PBE, with double ξ-plus-polarization (DZP) basis sets and a real space mesh cutoff of 200 Ry.

Results and Discussion

Structure and energetics of boron, vacancy, and boron-vacancy pair.— We first determined minimum-energy configurations for a substitutional B (B_s), a vacancy (*V*), and a B_s-*V* pair in armchair (*n*,*n*) CNTs with different tube diameters (5.6 Å $\leq D \leq$ 9.6 Å), and also examined how the thermal stability of a B_s-*V* pair with respect to B_s and *V* varies with tube diameter.

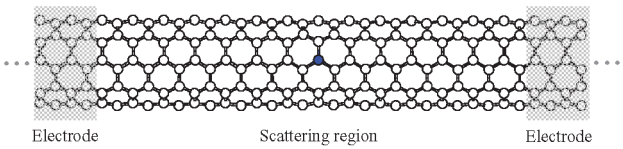

Figure 1. (Color online) Model CNT system employed in electronic transport calculations, consisting of a central scattering region and two semi-infinite electrodes (shaded in gray). Impurities and defects are placed at the center of the scattering region; shown here is a (5,5) CNT with a substitutional boron (in blue).

[z]E-mail: gshwang@che.utexas.edu

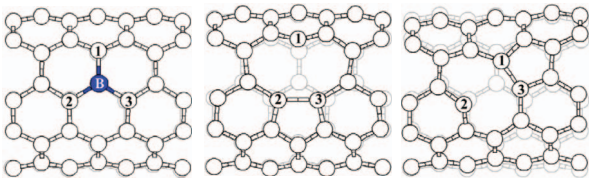

Figure 2. (Color online) Fully relaxed configurations for substitutional B [(a); B_s] and single V with a weak C-C bond along the axial [(b); V_a] and the diagonal [(c); V_d] direction in (5,5) CNT; Each background lattice (in light gray) represents the pristine (5,5) CNT, for comparison. White and black (blue) balls represent C and B atoms, respectively.

Substitutional boron (B_s).—For a small-diameter CNT, the substitutional B atom is displaced outward from the tube wall, due primarily to its larger covalent radius compared to C.[8] For the (5,5) CNT [Fig. 2a], the outward displacement is predicted to be about 0.2 Å, and the B-C bond lengths are $d_{B\text{-}C1} = 1.52$ Å and $d_{B\text{-}C2} = d_{B\text{-}C3} = 1.51$ Å in the radial and diagonal directions, respectively; note that the B-C bond lengths are greater than 1.43 Å as predicted for the C-C bond length in the pristine (5,5) CNT, in good agreement with previous studies.[8,9]

Single vacancy (V).—For a single vacancy, removal of one lattice C atom yields three unsaturated C atoms. Successive symmetry-lowering lattice relaxation causes two adjacent C atoms to form a weak covalent bond while the remaining C atom has one dangling bond. The weak C-C bonding can occur in two different orientations, one along the tube axis [*C2-C3*, Fig. 2b] and the other diagonal with respect to the tube axis [*C1-C3*, Fig. 2c];[28] the former and latter configurations are referred to as V_a and V_d, respectively, throughout the paper.

In an armchair CNT, the C-C bond preferentially forms in the diagonal direction due to a lesser structural constraint in the radial direction compared to the axial direction;[18,28] note that for the (5,5) CNT (with a diameter of $D \approx 6.9$Å) the C-C bond in the diagonal direction ($d_{C1\text{-}C3} = 1.55$ Å) is shorter than that in the axial direction ($d_{C2\text{-}C3} = 1.74$ Å). For the tube curvature, our DFT-GGA calculations predict the V_a and V_d formation energies to be 6.57 eV and 5.57 eV, respectively, in good agreement with previous calculations.[18,28] Here, the vacancy formation energy is given by:

$$E_f(V) = E_V - (N-1) \times E_{CNT}/N, \quad [1]$$

where E_V and E_{CNT} represent the total energies of the N-atom CNT with a vacancy and the pristine CNT, respectively.

B_s-V pair.—Figure 3 shows possible B_s-V configurations we examined. A single V can be placed at two different places adjacent to B_s; one at the radial [site 1 in Fig. 2a] and the other at the diagonal direction [site 2 (or 3) in Fig. 2a]. Our calculations show that the B atom would be either two, three, or fourfold coordinated. If the vacancy is located at site 1 [Fig. 2a], the B atom would have twofold coordination with the weak bond formation between two unsaturated C atoms in the axial direction (*C4-C9*) [$B_s(Di)$-V_a, Fig. 3a], threefold coordination with the formation of a weak B-C bond (*B-C4*) in the diagonal direction [$B_s(Tr)$-V_a, Fig. 3b], or fourfold coordination with the B atom moving radially to a more central location and bonding with all four neighboring C atoms [$B_s(Te)$-V_a, Fig. 3c]. Among these three structures, the threefold $B_s(Tr)$-V_a turns out to be the most energetically favorable configuration in the (5,5) CNT. The relative formation energies of the $B_s(Di)$-V_a, $B_s(Tr)$-V_a and $B_s(Te)$-V_a pairs with respective to B_s are predicted to be 6.10 eV, 4.48 eV, and 4.58 eV, respectively; the formation energy is given by

$$E_f(B_s\text{-}V) = E_{BV} - (E_B - E_{CNT}/N), \quad [2]$$

where E_{BV}, E_B, and E_{CNT} are the total energies of the N-atom CNTs with a B_s-V pair, a B_s, and no defect/impurity, respectively.

If the vacancy is located at site 2 [Fig. 2a], the B atom would be twofold or fourfold coordinated. In the twofold configuration, a

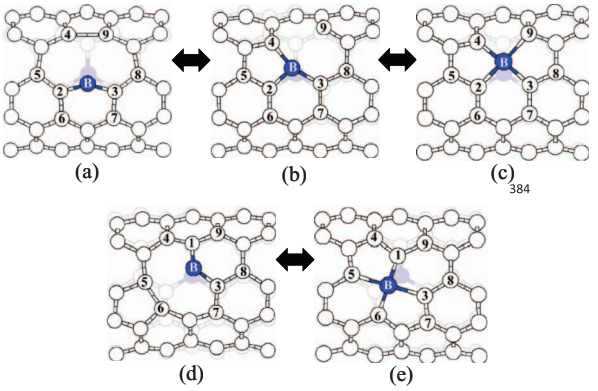

Figure 3. (Color online) Fully relaxed configurations for a B-V pair in different minimum-energy configurations. (Upper panels) a single V is located at *C1* [in Fig. 2a]; the B atom could be twofold [(a), $B_s(Di)$-V_a], threefold [(b), $B_s(Tr)$-V_a], or fourfold [(c), $B_s(Te)$-V_a] coordinated. (Lower panels) a single V is located at *C2* [in Fig. 2a]; the B atom could be twofold [(d), $B_s(Di)$-V_d] or fourfold [(e), $B_s(Te)$-V_d] coordinated. Each background lattice (in light gray) represents a (5,5) CNT with substitutional B. White and black (blue) balls represent C and B atoms, respectively.

weak C-C bond (*C5-C6*) is formed in the diagonal direction [$B_s(Di)$-V_d, Fig. 3d]. Unlike the $B_s(Tr)$-V_a case, the threefold B configuration [$B_s(Tr)$-V_d] is unstable and spontaneously transforms to the energetically more favorable fourfold configuration [$B_s(Te)$-V_d, Fig. 3e]. In the $B_s(Te)$-V_d case, the B atom moves diagonally to bond with all four neighboring C atoms; two of the B-C bonds (*B-C1* and *B-C6*) are approximately in the radial direction and the remaining two (*B-C3* and *B-C5*) are approximately in the axial direction. In the distorted tetrahedral structure, the radial B-C bonds ($d_{B\text{-}C1} = d_{B\text{-}C6} = 1.64$ Å) are noticeably shorter than their axial counterparts ($d_{B\text{-}C3} = d_{B\text{-}C5} = 1.83$ Å). The relative formation energies for $B_s(Di)$-V_d and $B_s(Te)$-V_d are 4.55 eV and 3.94 eV, respectively.

According to the calculation results, the fourfold $B_s(Te)$-V_d configuration tends to be the lowest-energy structure for a BV pair in the (5,5) CNT. Taking the formation energies of $B_s(Te)$-V_d (= 3.94 eV) and V_d (= 5.57 eV) (i.e., for the most stable B_s-V and V configurations), the energy gain from the B_s-V pairing with respect to fully separated B_s and V is estimated to be 1.63 eV. Given its high stability, the formation of $B_s(Te)$-V_d is very likely when B_s and V coexist in a CNT.

Tube diameter effect.—We examined how the structure and stability of B_s, V, and B_s-V are affected by the tube diameter for (n,n) armchair CNTs ($4 \le n \le 7$, corresponding to 5.6 Å $\le D \le$ 9.6 Å). Table I summarizes the variations in selected C-C/C-B bond lengths and C-B-C bend angles with the CNT diameter, together with the graphene case (infinite diameter limit) for comparison. As the tube diameter increases, the C-C bond distance $d_{C1\text{-}C3}$ in V_d increases from 1.53 Å to 1.58 Å, in good agreement with other calculation result.[28] For B_s, the B-C distances remain relatively constant with tube diameter.

For the B_s-V pair, the diameter dependence of bond lengths and bend angles varies with its geometry. Looking at the B_s-V_a case, the twofold $B_s(Di)$-V_a configuration is only stable for small diameter tubes ($n = 4, 5$) and easily converts to the fourfold $B_s(Te)$-V_a configuration for larger diameters ($n \ge 6$). It is worth noting that for the (5,5) tube the $B_s(Di)$-V_a configuration [Fig. 3a] yields a large C-B-C bend angle ($\angle_{C2\text{-}B\text{-}C3} = 139^\circ$) and a short B-C bond length ($d_{B\text{-}C2} = d_{B\text{-}C3} = 1.41$ Å); it has structural similarity with borabenzene ($\angle_{C\text{-}B\text{-}C} = 143^\circ$ and $d_{B\text{-}C} = 1.43$ Å from our calculations) in which the B atom is highly unstable and acts as a Lewis acid center.[29] As the tube diameter increases, the axial bond ($d_{C4\text{-}C9}$) weakens, thereby allowing the electrophilic B to bond with the two C atoms to be fourfold coordinated in tubes with n $\ge$ 6. In the threefold $B_s(Tr)$-V_a configuration, the length of weak B-C bonds [$d_{B\text{-}C4}$ in Fig. 3b] increases from 1.63 Å ($n = 4$) to 1.69 Å ($n = 7$) with increasing the tube diameter; at the same time, the dis-

Table I. Selected C-C and C-B bond lengths (d) and C-B-C bend angles ($\angle$) for relaxed B_s, V, B_s-V geometries for different tube sizes [(n, n) CNTs; n = 4–7, corresponding to D = 5.6–9.6 Å]. For comparison, the corresponding bond lengths and bend angles in flat graphene (Gr) are also listed. The bond lengths and bend angles are given in Å and degree (°), respectively. See Figs. 2 and 3 for the atom labels.

	B_s	V_a	V_d	$B_s(Di)$-V_a		$B_s(Tr)$-V_a	$B_s(Te)$-V_a		$B_s(Di)$-V_d		$B_s(Te)$-V_d	
(n,n)	$d_{B\text{-}C1}$	$d_{C2\text{-}C3}$	$d_{C1\text{-}C3}$	$d_{C4\text{-}C9}$	$\angle_{C2\text{-}B\text{-}C3}$	$d_{B\text{-}C4}$	$d_{B\text{-}C2}$	$\angle_{C2\text{-}B\text{-}C9}$	$d_{C5\text{-}C6}$	$\angle_{C1\text{-}B\text{-}C3}$	$d_{B\text{-}C1}$	$\angle_{C1\text{-}B\text{-}C6}$
D	$d_{B\text{-}C2}$					$d_{B\text{-}C9}$	$d_{B\text{-}C3}$	$\angle_{C3\text{-}B\text{-}C4}$			$d_{B\text{-}C3}$	$\angle_{C3\text{-}B\text{-}C5}$
(4,4)	1.53	1.68	1.53	1.70	137	1.63			1.55	116	1.63	125
5.6 Å	1.51					2.60					1.83	164
(5,5)	1.52	1.74	1.55	1.83	139	1.66	1.81	168	1.57	119	1.64	131
6.9 Å	1.51					2.50	1.66	163			1.83	162
(6,6)	1.52	1.78	1.57			1.68	1.81	166	1.59	119	1.65	137
8.2 Å	1.51					2.41	1.67	163			1.83	161
(7,7)	1.51	1.80	1.58			1.69	1.80	164	1.60	120	1.66	140
9.6 Å	1.50					2.32	1.68	163			1.82	160
Gr	1.49	1.99					$d_{B\text{-}C}$ = 1.79					
∞							$\angle_{C\text{-}B\text{-}C}$ = 162					

tance between the B and twofold-coordinated C ($d_{B\text{-}C9}$) decreases from 2.60 Å to 2.32 Å. As $d_{B\text{-}C9}$ decreases, the strain energy required to form the fourth B-C bond decreases relative to the energy gained through the B-C bond formation. Thus, like the twofold $B_s(Di)$-V_a case, the threefold $B_s(Tr)$-V_a becomes unfavorable with tube diameter, as compared to the fourfold $B_s(Te)$-V_a, and cannot exist stably in a nearly flat geometry (the graphene limit). On the other hand, the fourfold $B_s(Te)$-V_a structure is hardly formed for small diameter nanotubes ($n < 5$). In the $B_s(Te)$-V_a case [see Fig. 3c], it is energetically favorable for the two of the four B-C bonds (*B-C3* and *B-C4*) to be shorter than the other two (*B-C2* and *B-C9*). This symmetry breaking results in an energy gain from the formation of the two stronger bonds relative to the strain energy associated with the lattice distortion. As the tube diameter increases, the length of the short B-C bonds ($d_{B\text{-}C3}$ and $d_{B\text{-}C4}$) increases while that of the longer B-C bonds ($d_{B\text{-}C2}$ and $d_{B\text{-}C9}$) remain nearly unchanged; all B-C bond lengths become equal (= 1.79 Å) in the flat graphene sheet.[30]

For the case of B_s-V_d, the C-C bond length ($d_{C5\text{-}C6}$) of the twofold $B_s(Di)$-V_d [see Fig. 3d] increases from 1.55 Å to 1.60 Å as the tube diameter increases from $n = 4$ to $n = 7$. In spite of the elongation, the C-C bond in the diagonal direction [*C5-C6* in Fig. 3d] tends to be stronger than that in the axial direction [*C4-C9* in Fig. 3a]. As such, the twofold structure likely exists stably for $n > 5$ even though the B-C distances ($d_{B\text{-}C5}$ and $d_{B\text{-}C6}$) get shorter; in the flat graphene sheet, however, the increased B-C interaction leads to its transformation with no significant barrier (≈ 0.06 eV) into the more stable fourfold $B_s(Te)$-V_d structure.[30] For the fourfold $B_s(Te)$-V_d structure, the distorted tetrahedral configuration is likely maintained in large-diameter CNTs; the length of the radial B-C bonds [$d_{B\text{-}C1}$ and $d_{B\text{-}C6}$ in Fig. 3e] increases from 1.63 Å ($n = 4$) to 1.66 Å ($n = 7$) while that of the axial B-C bonds ($d_{B\text{-}C3}$ and $d_{B\text{-}C5}$) remains nearly unchanged at 1.83 Å. Even in graphene, the fourfold B tends to adopt a distorted tetrahedral configuration where the neighboring C atoms are displaced by ±0.27 Å perpendicular to the graphene plane.[30] This might be attributed to the tendency that the fourfold B favors a tetrahedral (sp^3) structure as opposed to square-planar (sp^2);[31] however, due to the rest of the in-plane C lattice, a perfect tetrahedron (having C-B-C angles of 109°) is highly unlikely to form.

Figure 4a summarizes the calculated formation energies of V and B_s-V at various configurations in terms of tube diameter. For all tube diameters examined, the fourfold $B_s(Te)$-V_d remains the most energetically favorable, while the formation energies increase monotonically with tube diameter. For a single V, the weak C-C bond is stretched with tube diameter (approaching 1.99 Å in graphene as opposed to 1.42 Å for a C-C bond in pristine graphene), leading to the increase of the vacancy formation energy. A similar effect is observed with the BV pair; however, in the $B_s(Te)$-V_d configuration, the weakening of the shorter B-C bond is less significant. Consequently, the $B_s(Te)$-V_d formation energy increases less rapidly with tube diameter compared to the single V case, and thus the binding energy of the $B_s(Te)$-V_d pair increases and can be as high as 2.5 eV in graphene [see Fig. 4b].

Electronic Structure and Electrical Conductance.— We now turn to examine how the B_s-V pairing modifies the electronic and charge transport properties of CNTs, as compared to the B_s and V cases which have been well studied in the past decade.[16–18] Figures 5–7 show calculated spin-polarized conductances for (5, 5) armchair CNTs with B_s, V_d, and $B_s(Te)$-V_d, respectively; in each plot, the corresponding conductance of an defect-free (5, 5) CNT is also presented as a broken line.

In a pristine armchair CNT, two energy bands originating from the π and π* states intersect at the Fermi level (E_F),[16] rendering two conducting channels and consequently inducing a conductance (per spin) of $2g_0$ ($= 2e^2/h$) in the vicinity of E_F [i.e., E_F–1.5 eV < E < E_F + 1.2 eV in the (5, 5) CNT]. The presence of defects or impurities leads to a reduction in conductance due to resonant backscattering. For B_s

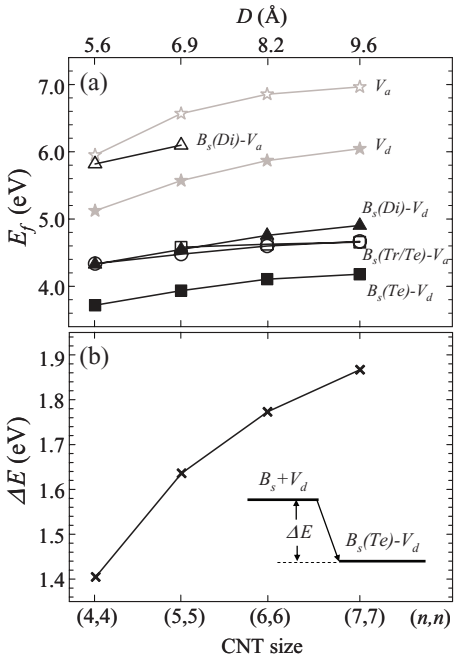

Figure 4. (a) Relative formation energies (E_f) with respect to substitutional B for single V and B_s-V pair in different configurations (refers to Figs. 2 and 3 for the V and B-V labels) and (b) binding energies (ΔE) for $B_s(Te)$-V_d with respect to fully separated B_s and V_d, as a functions of tube size [(n,n) = tube index, D = diameter].

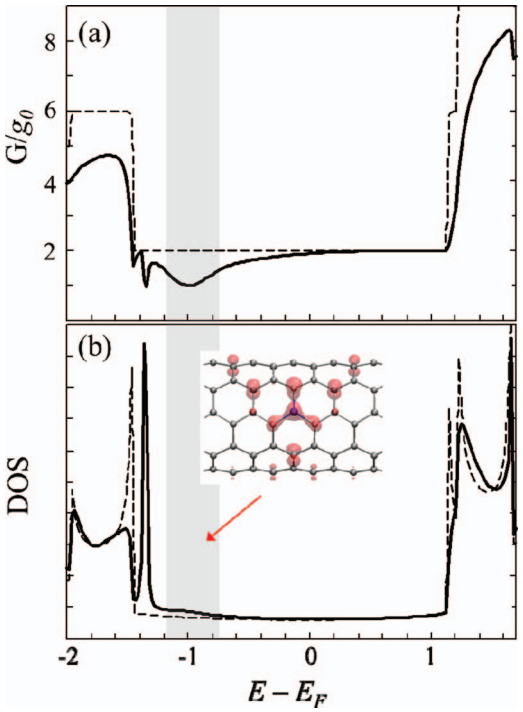

Figure 5. (Color online) (a) Calculated spin-polarized conductance and (b) total DOS for (5,5) CNT with a B_s. Here, the spin-up and spin-down states are degenerate. The inset [in (b)] shows the band-decomposed charge density (with isosurface value of 0.003) within -1.22 eV $< E$–$E_F < -0.74$ eV (shaded in gray), responsible for the corresponding broad dip as shown in (a); C and B atoms are indicated by gray and black (blue) balls, respectively. For comparison, the conductance and total DOS of pristine (5,5) CNT are also presented as broken lines.

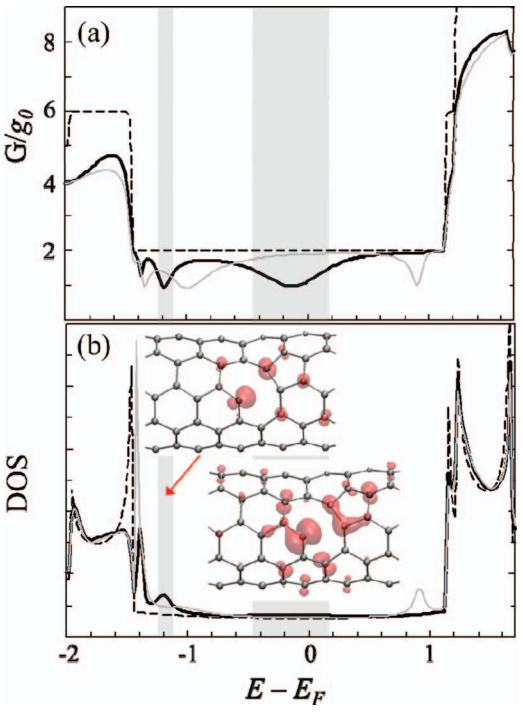

Figure 6. (Color online) (a) Calculated spin-polarized conductance and (b) total DOS of (5,5) CNT with a V_d. The black and gray solid lines indicate the majority (spin-up) and minority (spin-down) states, respectively. The insets [in (b)] show the band-decomposed charge density (for the majority state with isosurface value of 0.003) within -1.26 eV $< E - E_F < -1.07$ eV and -0.50 eV $< E$–$E_F < 0.17$ eV (shaded in gray), causing the corresponding narrow and broad conductance dips [(a)]. For comparison, the conductance and total DOS of pristine (5,5) CNT are also presented as broken lines.

(in Fig. 5), while the up and down spin states are nearly degenerate, the conductance per spin drops from $2g_0$ to g_0 at E_F–1.0 eV and E_F–1.4 eV and remains unchanged above E_F. The conductance dips are attributed to the quasibound states induced by the B impurity as demonstrated by the electron density of states (DOS) [Fig. 5b] and the corresponding band-decomposed charge densities (that clearly show the existence of the loosely bound π states in the vicinity of B) [see inset of Fig. 5b].

Our calculations predict that the minimum-energy configuration of V_d has a finite net magnetic moment ($\mu \approx 0.69\ \mu_B$). While the spin states are no longer degenerate, the conductance in Fig. 6a shows dips at E_F–1.4 eV, E_F–1.2 eV, and E_F–0.1 eV for the majority spin and E_F–1.4 eV, E_F–1.0 eV, and E_F+0.9 eV for the minority spin. As stated earlier, the single V structure has an unsaturated C atom while two adjacent C atoms form a weak covalent bond; the σ-orbital on the unsaturated atom is rather strongly localized in nature. The localized σ-orbital and quasilocalized π-orbitals are responsible for the relatively narrow and wide dips, respectively, as can be seen in the DOS and band-decomposed charge density plots [Fig. 6b].

Upon the formation of the most favorable B_s*(Te)*-V_d pair that has zero net magnetic moment, the conductance [in Fig. 7a] exhibits similarity to the B_s case [in Fig. 5a] while most of the vacancy features likely disappear. This is not surprising considering that the fourfold coordinated B atom likely acts like an acceptor, leading to perturbation of the nearby π states which may cause the wide dip at E_F–0.9 eV [see Fig. 7a]. Unlike the B_s case, an additional narrow dip occurs at $E_F + 1.1$ eV. The conductance drop is likely attributed to the σ states of the four C neighbors as demonstrated by the DOS and corresponding band decomposed charge density analysis [Fig. 7b]; Note that the highly distorted tetrahedral BC_4 structure may inhibit the formation of complete single covalent B-C bonds through sp^3 hybridization, as pointed out by a recent theoretical study.[30]

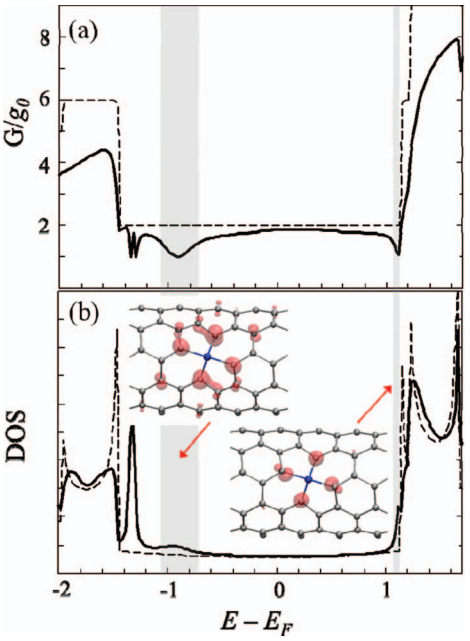

Figure 7. (Color online) Calculated spin-polarized conductance and (b) total DOS of (5,5) CNT with a B-V in the B_s*(Te)*-V_d configuration. Here, the spin-up and spin-down states are degenerate. The insets [in (b)] show the band-decomposed charge density (with isosurface value of 0.003) within -1.08 eV $< E$–$E_F < -0.69$ eV and 1.05 eV $< E$–$E_F < 1.13$ eV (shaded in gray), causing the corresponding broad and narrow conductance dips [(a)]; C and B atoms are indicated by gray and black (blue) balls, respectively. For comparison, the conductance and total DOS of pristine (5,5) CNT are also presented as broken lines.

Summary

DFT-GGA calculations were performed to examine the formation, structure, and stability of a boron-vacancy (B-V) pair in armchair (n, n) CNTs with different diameters ($n = 4$–7, corresponding to $D = 5.6$–9.6Å). While the B atom in a B-V pair can be two, three, or fourfold coordinated, the fourfold state that saturates the V dangling bonds turns out to be energetically more favorable than the others. The fourfold B tends to adopt a distorted tetrahedral configuration, attributed to its tendency to favor a tetrahedral (sp^3) structure as opposed to square-planar (sp^2). For a small (5,5) tube, the energy gain due to B-V pairing with respect to fully separated B and V is predicted to be 1.63 eV. The B-V formation energy increases with tube diameter, but less rapidly than the single V case; as a consequence, the binding energy of a B-V pair increases and can be as high as 2.5 eV in flat graphene. The high binding strength suggests B-V pair formation to be very likely when B and V coexist in CNTs. The structural changes of B, V, and B-V with tube diameter are described in detail. Using NEGF combined with DFT, we also examined the influence of B-V pairing on the charge transport properties of CNTs with comparisons to the isolated B and V cases. For substitutional B, conductance dips appear at E_F–1.0 eV and E_F–1.4 eV due to loosely bound π states in the vicinity of B; whereas a single V defect induces conductance drops at E_F–1.4 eV, E_F–1.2 eV, and E_F–0.1 eV for the majority spin and E_F–1.4 eV, E_F–1.0 eV, and E_F+0.9 eV for the minority spin, while localized σ-orbital and quasilocalized π-orbitals are responsible for the relatively narrow and wide dips. Upon B-V pair formation, the vacancy features mostly disappear while the B features are preserved, suggesting possible 'pseudo-annihilation' of V defects, particularly for charge transport, in B-doped CNTs. The fundamental findings would assist in better understanding the effect of impurities and defects on the electronic properties of CNTs.

Acknowledgments

This work was supported by the R. A. Welch Foundation (F-1535). The authors also thank the Texas Advanced Computing Center for use of their computing resources.

References

1. S. M. M. Dubois, Z. Zanolli, X. Declerck, and J. C. Charlier, *Eur. Phys. J. B*, **72**, 1 (2009).
2. P. R. Bandaru, C. Daraio, S. Jin, and A. M. Rao, *Nat. Mater.*, **4**, 663 (2005).
3. J. Kong, N. R. Franklin, G. Zhou, M. G. Chapline, S. Peng, K. Cho, and H. Dai, *Science*, **287**, 622 (2000).
4. Savas Berber, Y. Kwon, and D. Tománek, *Phys, Rev. Lett.*, **84**, 4613 (2000).
5. D. L. Carroll, Ph. Redlich, X. Blase, J. C. Charlier, S. Curran, P. M. Ajayan, S. Roth, and M. Rühle, *Phys. Rev. Lett.*, **81**, 2332 (1998).
6. A. H. Nevidomskyy, G. Csányi, and M. C. Payne, *Phys. Rev. Lett.*, **91**, 105502 (2003).
7. Y. Yagi, T. M. Briere, M. H. F. Sluiter, V. Kumar, A. A. Farajian, and Y. Kawazoe, *Phys. Rev. B*, **69**, 075414 (2004).
8. J. Yi and J. Bernholc, *Phys. Rev. B*, **47**, 1708 (1993).
9. T. Koretsune and S. Saito, *Phys. Rev. B*, **77**, 165417 (2008).
10. R. Singh and P. Kroll, *J. Phys.: Condens. Matter*, **21**, 196002 (2009).
11. L. Bai and Z. Zhou, *Carbon*, **45**, 2105 (2007).
12. Z. Zhou, X. Gao, J. Yan, D. Song, and M. Morinaga, *Carbon*, **42**, 2677 (2004).
13. M. Sankaran and B. Viswanathan, *Carbon*, **45**, 1628 (2007).
14. C. Jin, K. Suenaga, and S. Iijima, *Nano Lett.*, **8**, 1127 (2008).
15. A. V. Krasheninnikov and F. Banhart, *Nat. Mater.*, **6**, 723 (2007).
16. H. J. Choi, J. Ihm, S. G. Louie, and M. L. Cohen, *Phys. Rev. Lett.*, **84**, 2917 (2000).
17. A. R. Rocha, J. E. Padilha, A. Fazzio, and A. J. R. da Silva, *Phys. Rev. B*, **77**, 153406 (2008).
18. Z. Zanolli and J. C. Charlier, *Phys. Rev. B*, **81**, 165406 (2010).
19. A. V. Krasheninnikov, P. O. Lehtinen, A. S. Foster, and R. M. Nieminen, *Chem. Phys. Lett.*, **418**, 132 (2006).
20. J. P. Perdew, K. Burke, and M. Ernzerhof, *Phys. Rev. Lett.*, **77**, 3865 (1996).
21. G. Kresse and J. Furthmuller, *VASP the Guide*, Vienna University of Technology, Vienna, 2001.
22. P. E. Blöchl, *Phys. Rev. B*, **50**, 17953 (1994).
23. H. J. Monkhorst and J. D. Pack, *Phys. Rev. B*, **13**, 5188 (1976).
24. M. Brandbyge, J. Mozos, P. Ordejón, J. Taylor, and K. Stokbro, *Phys. Rev. B*, **65**, 165401 (2002); J. M. Soler, E. Artacho, J. Gale, D. A. Garcia, J. Junquera, P. Ordejón, and D. Sánchez-Portal, *J. Phys.: Condens. Matter*, **14**, 2745 (2002).
25. R. Landauer, *Philos. Mag.*, **21**, 863 (1970).
26. Y. Meir and N. S. Wingreen, *Phys. Rev. Lett.*, **68**, 2512 (1992).
27. S. Datta, *Electronic Transport in Mesoscopic Systems*, Cambridge University Press, 1995.
28. A. J. Lu and B. C. Pan, *Phys. Rev. Lett.*, **92**, 105504 (2004).
29. J. Cioslowski and P. J. Hay, *J. Am. Chem. Soc*, **112**, 1707 (1990).
30. K. E. Kweon and G. S. Hwang, *Phys. Rev. B*, **82**, 195439 (2010).
31. A. I. Boldyrev and O. P. Charkin, *J. Struc. Chem.*, **26**, 451 (1985).